Exploring the nonlinear regime of light-matter interaction using electronic spins in diamond

Nir Alfasi,[1] Sergei Masis,[1] Roni Winik,[1] Demitry Farfurnik,[2] Oleg Shtempluck,[1] Nir Bar-Gill,[2] and Eyal Buks[1]
[1]*Andrew and Erna Viterbi Department of Electrical Engineering, Technion, Haifa 32000, Israel*
[2]*Racah Institute of Physics, The Hebrew University of Jerusalem, Jerusalem 9190401, Israel*

(Received 14 November 2017; published 7 June 2018)

The coupling between defects in diamond and a superconducting microwave resonator is studied in the nonlinear regime. Both negatively charged nitrogen-vacancy and $P1$ defects are explored. The measured cavity mode response exhibits strong nonlinearity near a spin resonance. Data is compared with theoretical predictions and a good agreement is obtained in a wide range of externally controlled parameters. The nonlinear effect under study in the current paper is expected to play a role in any cavity-based magnetic resonance imaging technique and to impose a fundamental limit upon its sensitivity.

DOI: 10.1103/PhysRevA.97.063808

I. INTRODUCTION

Cavity quantum electrodynamics (CQED) [1] is the study of the interaction between photons confined in a cavity and matter. CQED has applications in a variety of fields, including magnetic resonance imaging and quantum computation [2]. The CQED interaction can be probed by measuring the response of a cavity mode. Commonly, the effect of matter on the response diminishes as the energy stored in the cavity mode under study is increased [3]. This nonlinear effect, which is the focus of the current study, imposes a severe limit upon the performance of a variety of CQED systems.

In the current study, we explore the nonlinear CQED interaction between defects in a diamond crystal and a superconducting microwave cavity (resonator) having a spiral shape [4]. Two types of defects are investigated: a negatively charged nitrogen-vacancy NV^- defect and a nitrogen 14 (nuclear spin-1) substitutional defect ($P1$). Strong coupling between defects in the diamond and a superconducting resonator has been demonstrated at ultralow temperatures [5–11]; however, the regime of nonlinear response was not addressed. In this study, we find that the cavity response becomes highly nonlinear near a CQED resonance. In addition, for the case of NV^- defects, the response is strongly affected by applying optically induced spin polarization (OISP). The experimental findings are compared with theory and good agreement is obtained.

II. EXPERIMENTAL SETUP

The experimental setup is schematically depicted in Fig. 1(a). Defects in a [100]-type Ib diamond are created using 2.8 MeV electron irradiation with a dose of approximately $8 \times 10^{18} e/\mathrm{cm}^2$, followed by annealing at 800 °C for 8 hours and acid cleaning, resulting in the formation of NV^- defects with density of 1.23×10^{17} cm^{-3} [12]. The diamond wafer is then placed on top of a sapphire wafer supporting a superconducting spiral resonator made of niobium [see Fig. 1(b)]. Externally applied magnetic field $\mathbf{B}$ is employed for tuning the system into a CQED resonance. A coaxial cable terminated by a loop antenna (LA) transmits both injected and off-reflected microwave signals. The LA has a coupling given by $\gamma_f/2\pi = 0.367$ MHz to the spiral's fundamental mode, which has a frequency of $\omega_c/2\pi = 2.53$ GHz and an unloaded damping rate of $\gamma_c/2\pi = 0.253$ MHz [these values are extracted from a fitting based on Eq. (7) below]. All measurements are performed at a base temperature of $T = 3.1$ K. A network analyzer (NA) measurement of the temperature dependence of the resonance line shape is seen in Fig. 1(c). The color-coded plot depicts the reflectivity coefficient $R_c = P_r/P_p$ in dB units, where $P_p = -70$ dBm and P_r are, respectively, the injected power into the LA and the off-reflected power from the LA, as a function of both frequency of injected signal $\omega_p/2\pi$ and temperature T. Laser light of wavelength $\lambda_L = 532$ nm and intensity I_L (in units of power per unit area) is injected into the diamond wafer using a multimode optical fiber F1, and another multimode optical fiber F2 delivers the emitted photoluminescence (PL) to an optical spectrum analyzer [see Fig. 2(a)]. Numerical calculation is employed for evaluating the shape of the spiral's fundamental mode [see Fig. 1(d)].

III. CAVITY-BASED DETECTION OF MAGNETIC RESONANCE WITH NV CENTERS IN DIAMOND

The negatively charged NV^- defect in diamond consists of a substitutional nitrogen atom (N) combined with a neighbor vacancy (V) [13]. The ground state of the NV^- defect is a spin triplet having symmetry $^3A_2$ [14,15], composed of a singlet state $|m_e = 0\rangle$ and a doublet $|m_e = \pm 1\rangle$. The angular resonance frequencies $\omega_\pm$ corresponding to the transitions between the state $|m_e = 0\rangle$ and the states $|m_e = \pm 1\rangle$ are approximately given by [16–18]

$$\omega_\pm = D \pm \sqrt{\gamma_e^2 B_\parallel^2 + E^2} + \frac{3}{2}\frac{\gamma_e^2 B_\perp^2}{D}, \tag{1}$$

where $B_\parallel$ is the magnetic field component parallel to the axis of the NV defect and $B_\perp$ is the transverse one. The parameter $\gamma_e = 2\pi \times 28.03$ GHz T^{-1} is the electron spin gyromagnetic ratio. In the absence of strain and when the externally applied magnetic field vanishes, one has $\omega_\pm = D$, where $D = 2\pi \times 2.87$ GHz. Internal strain, however, may lift the degeneracy between the states $|m_e = -1\rangle$ and $|m_e = +1\rangle$, and give rise to

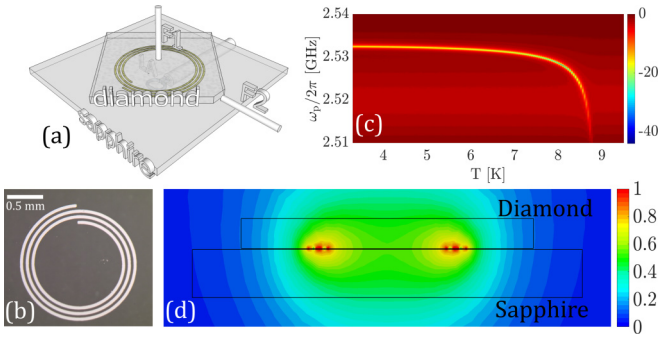

FIG. 1. The experimental setup. (a) A loop antenna (LA) is coupled to the spiral resonator. Two multimode optical fibers are coupled to the diamond wafer. Fiber F1 is employed for delivering laser light of wavelength $\lambda_L = 532$ nm, and fiber F2 probes the emitted photoluminescence (PL). (b) The spiral resonator has three turns, an inner radius of 0.59 mm, and an outer radius of 0.79 mm. (c) The resonance line shape of the spiral's fundamental mode vs temperature. (d) The magnetic induction magnitude $|\mathbf{B}_c(\mathbf{r})|$ of the fundamental mode vs position $\mathbf{r}$ in a plane perpendicular to both wafers that contains the center of the spiral.

a splitting given by $2E$ (in our sample, $E = 2\pi \times 10$ MHz). In a single-crystal diamond, the NV defects have four different possible orientations with four corresponding pairs of angular resonance frequencies $\omega_\pm$.

The technique of optical detection of magnetic resonance (ODMR) can be employed for measuring the resonance frequencies $\omega_\pm$ [19,20]. The measured PL spectrum is seen in Fig. 2(a). The integrated PL signal in the band 660–760 nm is plotted as a function of microwave input frequency $\omega_p/2\pi$ and externally applied magnetic field $|\mathbf{B}|$ in Figs. 2(b) and 2(c). In this measurement, the microwave input power is set to $P_p = 20$ dBm. The direction of the externally applied magnetic field $\mathbf{B}$ is found by fitting the measured ODMR frequencies $\omega_\pm$ with the calculated values given by Eq. (1).

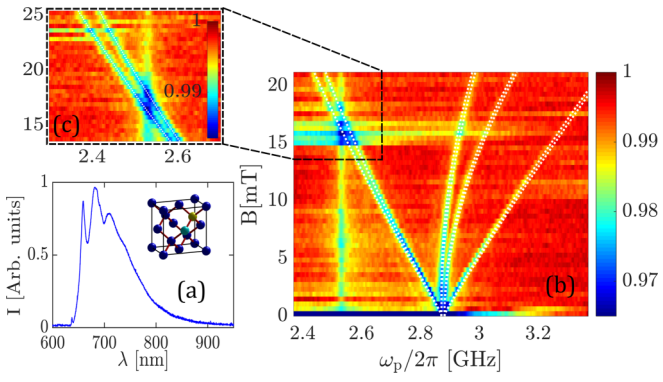

FIG. 2. ODMR. (a) The measured emitted PL spectrum. (b),(c) ODMR spectrum vs driving frequency $\omega_p/2\pi$ and magnetic field $|\mathbf{B}|$. The white dotted lines represent the frequencies $\omega_\pm/2\pi$ calculated using Eq. (1). The fitting procedure yields the direction of the magnetic field $\hat{\mathbf{b}}$, which is expressed as $\hat{\mathbf{b}} = T_{\hat{\mathbf{z}}}(\theta_z)T_{\hat{\mathbf{y}}}(\theta_y)T_{\hat{\mathbf{x}}}(\theta_x)\hat{\mathbf{z}}$, where $\hat{\mathbf{x}}$, $\hat{\mathbf{y}}$, and $\hat{\mathbf{z}}$ are unit vectors in the crystal directions [100], [010], and [001], respectively, and $T_{\hat{\mathbf{s}}}(\theta_s)$ is a rotation operator around the axis $\hat{\mathbf{s}}$, where $s \in \{x,y,z\}$. The rotation angles found from the fitting procedure are $\theta_x/\pi = -0.02$, $\theta_y/\pi = 0.002$, and $\theta_z/\pi = 0.05$.

The ODMR spectrum contains a profound resonance feature at the frequency of the spiral resonator, $\omega_c/2\pi = 2.53$ GHz [see Fig. 2(b)]. This feature is attributed to heating-induced change in the internal stress in the diamond wafer. Two (out of four) resonance frequencies $\omega_-/2\pi$ can be tuned close to the spiral resonator frequency $\omega_c/2\pi$ by setting the magnetic field $|\mathbf{B}|$ close to the value of 16 mT. The two groups of NV^- defects giving rise to these two resonances have the smallest angles with respect to the externally applied magnetic field (see caption of Fig. 2). In this region, which is magnified in Fig. 2(c), the deepest ODMR is obtained when the magnetic and resonator frequencies coincide.

The same two spin resonances seen in Fig. 2(c) can be detected without employing the technique of ODMR provided that their frequencies are tuned close to the spiral resonator frequency $\omega_c/2\pi$. The plots (D: $P1$; $L0$), (D: $P2$; $L0$), and (D: $P3$; $L0$) of Fig. 3 depict NA measurements of the microwave reflectivity coefficient R_c with three different values of the injected signal microwave power P_p. No laser light is injected into the diamond wafer in these measurements (labeled by $L0$ in Fig. 3). Henceforth, this method of spin detection is referred to as cavity-based detection of magnetic resonance (CDMR). Both CDMRs seen in Fig. 3 exhibit strong dependence on P_p, indicating thus that the interaction with the spins makes the cavity response highly nonlinear.

IV. SPIN-INDUCED NONLINEARITY

To account for the observed spin-induced nonlinearity, the experimental results are compared with theoretical predictions [21]. The decoupled cavity mode is characterized by an angular resonance frequency ω_c, Kerr coefficient K_c, linear damping rate γ_c, and cubic damping (two-photon absorption) rate G_c. The response of the decoupled cavity in the weak nonlinear regime (in which nonlinearity is taken into account to lowest nonvanishing order) can be described by introducing the complex and mode-amplitude-dependent cavity angular resonance frequency Υ_c, which is given by

$$\Upsilon_c = \omega_c - i\gamma_c + (K_c - iG_c)E_c, \tag{2}$$

where E_c is the averaged number of photons occupying the cavity mode. The imaginary part of Υ_c represents the effect of damping and the terms proportional to E_c represent the nonlinear contribution to the response.

The effect of the spins on the cavity response in the weak nonlinear regime is theoretically evaluated in [22]. The steady-state cavity mode response is found to be equivalent to the response of a mode having effective complex cavity angular resonance frequency $\Upsilon_{\rm eff}$ given by $\Upsilon_{\rm eff} = \Upsilon_c + \Upsilon_s$, where $\Upsilon_s = \sum_n \Upsilon_n$ and Υ_n, which represents the contribution of a spin labeled by the index n, and is given by (see Eq. (4) in [22])

$$\Upsilon_n = -\frac{g_n^2}{\Delta_n}\frac{1-\frac{i}{\Delta_n T_{2,n}}}{1+\frac{1+4g_n^2 T_{1,n}T_{2,n}E_c}{\Delta_n^2 T_{2,n}^2}}P_{zS,n}, \tag{3}$$

where g_n is the coupling coefficient between the nth spin and the cavity mode, $T_{1,n}$ and $T_{2,n}$ are the spin's longitudinal and transverse relaxation times, respectively, $\Delta_n = \omega_c - \omega_{s,n}$ is the frequency detuning between the cavity frequency ω_c

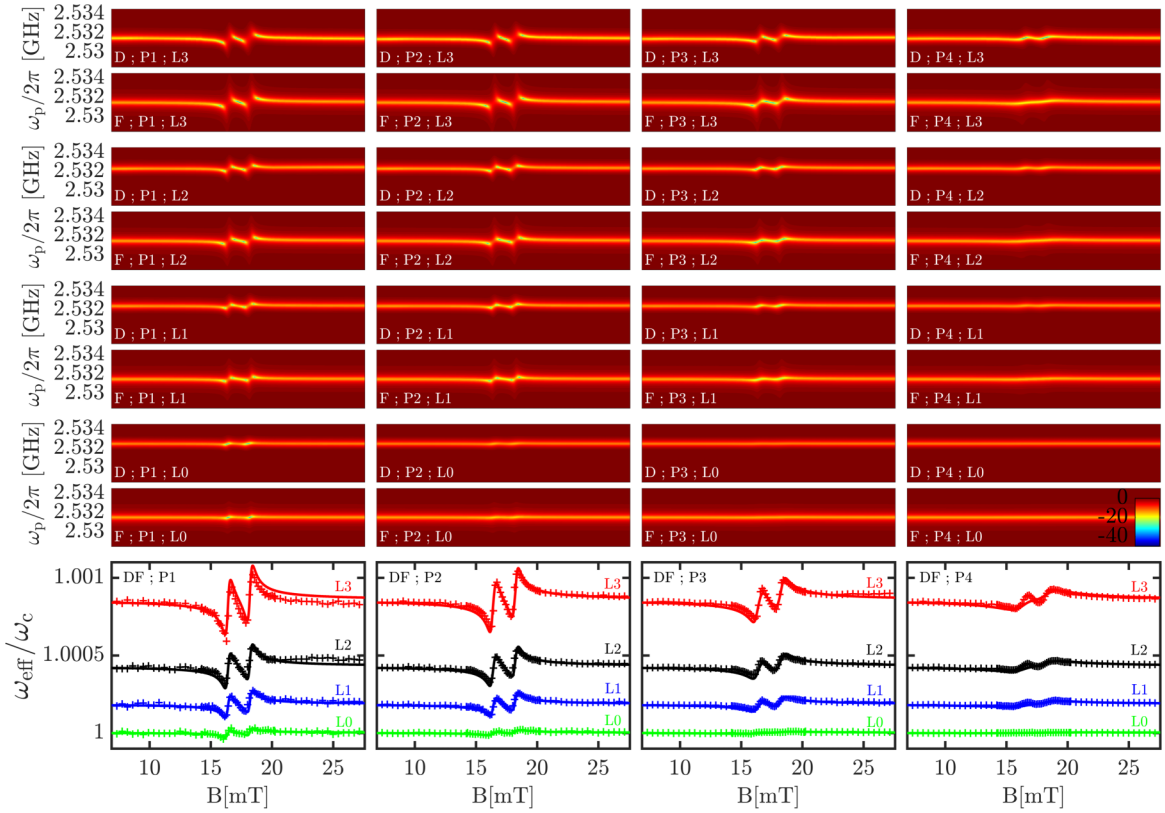

FIG. 3. Cavity mode reflectivity R_c with NV^- defects for various values of injected microwave power P_p ($P1 = -90$, $P2 = -70$, $P3 = -60$, and $P4 = -50$ dBm) and laser power I_L ($L0 = 0$, $L1 = 5.6$, $L2 = 12.8$, and $L3 = 30$ mW mm^{-2}). For each pair, the top plot is experimental data (labeled D) and the bottom is the theoretical prediction (labeled F). The bottom row shows the effective normalized resonance frequency (ω_{eff}/ω_c), which is obtained from the minimum reflectivity signal for each magnetic field, as a function of magnetic field. Each column corresponds to a single microwave power (DF; $P1$–$P4$) and each plot shows all four laser powers ($L3$ in red, $L2$ in black, $L1$ in blue, and $L0$ in green). Cross markers denote experimental data and solid lines represent theoretical predictions. Plots are vertically shifted for clarity. The parameters used for the calculation for the case of laser on (off) are $P_{zST} = -0.035$, $P_{zSO} = -0.55$, $\rho_s = 1.23 \times 10^{17}$ cm^{-3}, $T_2 = 219$ ns, $T_{1T} = 23$ ms ($T_{1T} = 565$ ms) [23] and $g_s/2\pi = 5.05$ Hz ($g_s/2\pi = 2.72$ Hz). The rate T_{1O}^{-1} of OISP is taken to be given by $T_{1O}^{-1} = 0.16 \times \gamma_O$, where $\gamma_O = I_L \sigma \lambda_L / hc$ is the rate of optical absorption, where $\sigma = 3 \times 10^{-17}$ cm^2 [24] is the optical cross section, h is the Plank's constant, and c is the speed of light in vacuum. The effective coupling coefficient g_s for both cases of laser on and off is calculated using Eq. (5) and the numerically calculated mode shape [see Fig. 1(d)]. The volume inside the diamond wafer illuminated by the laser is 0.76 mm^3.

and the spin's transition frequency $\omega_{s,n}$, and $P_{zS,n}$ is the spin's longitudinal polarization. The term proportional to E_c in the denominator of Eq. (3) gives rise to a nonlinear response.

The coupling coefficients g_n can be extracted from the numerically calculated magnetic field induction $\mathbf{B}_c(\mathbf{r})$ of the spiral's fundamental mode [see Fig. 1(d)] using the expression $g_n = \gamma_e |\mathbf{B}_c(\mathbf{r}_n)| \sin\varphi_n / E_c^{1/2}$ [6], where $\mathbf{B}_c(\mathbf{r}_n)$ is the cavity mode magnetic induction at the location of the spin $\mathbf{r}_n$ and φ_n is the angle between $\mathbf{B}_c(\mathbf{r}_n)$ and the NV axis. When all contributing spins share the same detuning factor Δ, polarization P_{zS}, and the same relaxation times T_1 and T_2, and when the variance in the distribution of g_n is taken into account to lowest nonvanishing order only, one finds that

$$\Upsilon_s = \frac{N_{eff} g_s^2}{\Delta} \frac{1 - \frac{i}{\Delta T_2}}{1 + \frac{1 + \frac{E_c}{E_{cc}}}{\Delta^2 T_2^2}}, \tag{4}$$

where $\rho_s(\mathbf{r})$ is the density of contributing NV^- defects, $N_{eff} = -\int d\mathbf{r} \rho_s P_{zS}$ is their effective number, the effective coupling coefficient g_s is given by

$$g_s^2 = \frac{\gamma_e^2 \mu_0 \hbar \omega_c \int d\mathbf{r} \rho_s |\mathbf{B}_c|^2 \sin^2\varphi P_{zS}}{\int d\mathbf{r} |\mathbf{B}_c|^2 \int d\mathbf{r} \rho_s P_{zS}}, \tag{5}$$

and $E_{cc} = (4 g_s^2 T_1 T_2)^{-1}$.

The underlying mechanism responsible for the spin-induced nonlinearity in the cavity mode response is attributed to the change in spin polarization that occurs via the cavity-mediated spin driving. As can be seen from Eq. (A83) of Ref. [22], the normalized change in polarization is proportional to the ratio E_c/E_{cc}. Consequently, the induced nonlinearity is expected to be negligibly small when $E_c \ll E_{cc}$ [as is also seen from Eq. (4)]. On the other hand, when $E_c \gg E_{cc}$, spin depolarization becomes saturated. In this limit, $\Upsilon_{eff} = \Upsilon_c + \Upsilon_s \simeq \Upsilon_c$ [see Eq. (4)], and, consequently, the cavity mode is expected to become effectively decoupled from the spins (this effective decoupling refers only to the averaged response, whereas noise properties remain affected by the spins). The regime of weak nonlinearity, in which nonlinearity can be taken into account to lowest nonvanishing order only, is discussed in Appendix.

Note, however, that in the current experiment, the nonlinearity can be considered as weak only in a narrow region, and most observations cannot be properly explained without accounting for higher-order nonlinear terms.

In general, the averaged number of photons E_c is found from the steady-state solution of the equations of motion that govern the dynamics of the system [22]. To lowest nonvanishing order in the coupling coefficient g_s, the effect of spins can be disregarded in the calculation of E_c. When, in addition, the intrinsic cavity mode nonlinearity, which is characterized by the parameters K_c and G_c, has a negligibly small effect, the number E_c can be approximated by the following expression (see Eq. (37) in [25]):

$$E_c = \frac{4\gamma_f P_p}{\hbar\omega_c} \frac{1}{(\omega_p - \omega_c)^2 + (\gamma_f + \gamma_c)^2}. \tag{6}$$

As can be seen from Eq. (4), $|\Upsilon_s|$ is a monotonically decreasing function of E_c. This suggests that the approximation in which Eq. (6) is employed for evaluating E_c (without taking into account both nonlinearity and the coupling to the spins) remains valid even when $4g_s^2 T_1 T_2 E_c \gg 1$, provided that intrinsic cavity mode nonlinearity remains sufficiently small. When intrinsic cavity mode nonlinearity can be disregarded, the cavity mode reflectivity R_c is given by [25]

$$R_c = \frac{(\omega_p - \Omega_c)^2 + (\gamma_f - \Gamma_c)^2}{(\omega_p - \Omega_c)^2 + (\gamma_f + \Gamma_c)^2}, \tag{7}$$

where the real frequencies Ω_c and Γ_c are related to the complex frequency Υ_{eff} by the relation $\Upsilon_{\text{eff}} = \Omega_c - i\Gamma_c$.

The fully analytical theoretical predictions given by Eqs. (4), (6), and (7) are employed for generating the plots (F: *P*1; *L*0), (F: *P*2; *L*0) and (F: *P*3; *L*0) of Fig. 3, which exhibit good agreement with the corresponding CDMR data plots (D: *P*1; *L*0), (D: *P*2; *L*0), and (D: *P*3; *L*0). The parameters that have been employed for the calculation are listed in the figure caption. These findings support the hypothesis that the above-discussed spin-induced nonlinearity is the underlying mechanism responsible for the suppression of electron spin resonance (ESR) at relatively high microwave input power P_p.

The CDMR data plots in Fig. 3 labeled *L*1, *L*2, and *L*3 are obtained from measurements with laser intensities 2.15, 12.8, and 30 mW mm^{-2}, respectively. As can be seen from the comparison to the plots labeled *L*0, in which the laser is turned off, the optical illumination strongly affects the measured cavity response.

The laser-induced change in the cavity response is attributed to the mechanism of OISP [23,26–29]. Spin is conserved in the optical dipole transitions between the triplet ground state $^3A_2$ of NV$^-$ and the triplet first excited state ^3E. However, transition from the spin states $m_e = \pm 1$ of ^3E to the ground state is also possible through an intermediate singlet states in a two-step nonradiative process. Such nonradiative process is also possible for the decay of the state $m_e = 0$ of ^3E; however, the probability of this process is about seven times smaller than the probability of nonradiative decay of the $m_e = \pm 1$ states [13]. The asymmetry between the decay of the $m_e = 0$ state, which is almost exclusively radiative, and the decay of the states $m_e = \pm 1$, which can occur via a nonradiative process, gives rise to OISP. For our experimental conditions, the probability to find any given NV$^-$ defect at any given time not in the triplet ground state $^3A_2$ is about 10^{-5} or less [13]. This fact is exploited below for taking the effect of OISP into account within the framework of a two-level model.

The effect of OISP can be accounted for by adjusting the values of the longitudinal relaxation time T_1 and longitudinal steady-state polarization P_{zS} and make them dependent on laser intensity I_L. The total rate of spin longitudinal damping γ_{s1} is given by [30]

$$\gamma_{s1} = -\frac{P_z - P_{zST}}{T_{1T}} - \frac{P_z - P_{zSO}}{T_{1O}}, \tag{8}$$

where the first term represents the contribution of thermal relaxation and the second one represents the contribution of OISP. Here, P_z is the instantaneous longitudinal polarization and T_{1T}^{-1} (T_{1O}^{-1}) is the rate of thermal relaxation (OISP). In the steady state and when $T_{1T}^{-1} \gg T_{1O}^{-1}$ (i.e., when OISP is negligibly small), the coefficient $P_{zST} = -\tanh(\hbar\omega_s/2k_B T)$ is the value of P_z in thermal equilibrium, where k_B is Boltzmann's constant and where T is the temperature. In the opposite limit of $T_{1O}^{-1} \gg T_{1T}^{-1}$ (i.e., when thermal relaxation is negligibly small), the coefficient P_{zSO} is the value of P_z in the steady state. Note that the total longitudinal damping rate γ_{s1} (8) can be expressed as $\gamma_{s1} = -T_1^{-1}(P_z - P_{zS})$, where $T_1^{-1} = T_{1T}^{-1} + T_{1O}^{-1}$ is the effective longitudinal relaxation rate, and the effective steady-state longitudinal polarization P_{zS} is given by $T_1^{-1} P_{zS} = T_{1T}^{-1} P_{zST} + T_{1O}^{-1} P_{zSO}$.

The theoretical expressions given above for T_1^{-1} and P_{zS} are employed for generating the plots labeled F of Fig. 3 for both cases of laser off (*L*0) and laser on (*L*1, *L*2, and *L*3). In spite of the simplicity of the model that is employed for the description of OISP, good agreement is obtained from the comparison with the CDMR data plots labeled D in a very wide range of values for the microwave power and laser intensity (the entire explored range of $P_p < 0$ dBm and $I_L < 30$ mW mm^{-2}). Note that no resonance splitting is observed in all CDMR measurements.

The line shapes of both ODMR and CDMR depend on the values of spin longitudinal T_1 and transverse T_2 damping times. In order to check consistency, we employ Eq. (2) of Ref. [31] in order to express the full width at half minimum (FWHM) $\Delta\nu$ of the ODMR in terms of T_1, T_2 and the driving amplitude, which is denoted by ω_1 (ω_1 coincides with the Rabi frequency at resonance). In the calculation of ω_1, it is assumed that the loop antenna can be treated as a perfect magnetic dipole. By substituting the damping times T_1 and T_2 that are listed in the caption of Fig. 3 into Eq. (2) of Ref. [31], one obtains $\Delta\nu = 14$ MHz, whereas the FWHM value extracted from the ODMR data using a fit to a Lorentzian is 13.5 MHz.

V. CAVITY-BASED DETECTION OF MAGNETIC RESONANCE WITH *P*1 CENTERS IN DIAMOND

A CQED resonance due to *P*1 defects [32,33] is observed when the externally applied magnetic field is tuned close to the value of 89 mT (see Fig. 4). When both the nuclear Zeeman shift and nuclear quadrupole coupling are disregarded, the spin Hamiltonian of a *P*1 defect is given by [9,34,35] $\mathcal{H} = \gamma_e \mathbf{B}\cdot\mathbf{S} + \hbar^{-1}A_\perp(S_x I_x + S_y I_y) + \hbar^{-1}A_\parallel S_z I_z$, where $\mathbf{S} = (S_x, S_y, S_z)$ is an electronic spin-1/2 vector operator, $\mathbf{I} = (I_x, I_y, I_z)$ is a nuclear spin-1 vector operator,

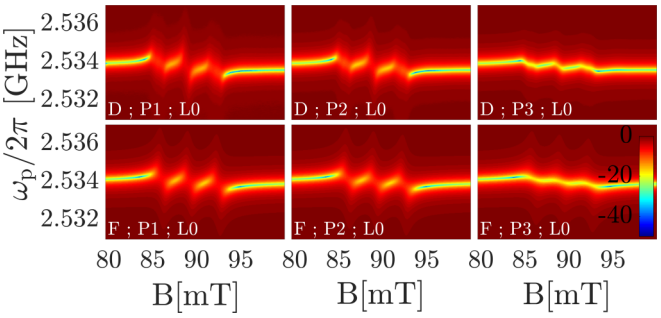

FIG. 4. Cavity mode reflectivity R_c with $P1$ defects for various values of injected microwave power P_p ($P1 = -90$, $P2 = -80$, and $P3 = -70$ dBm) with laser off. For each pair, the top plot is experimental data (labeled D) and the bottom is the theoretical prediction (labeled F). The parameters used for the calculation are $\gamma_c/2\pi = 0.304$ MHz, $\gamma_f/2\pi = 0.349$ MHz, $\rho_s = 1 \times 10^{18}$ cm^{-3}, $T_2 = 438$ ns, and $T_{1T} = 470$ ms [36]. The values of P_{zST} and g_s are the same as in Fig. 3 for the case of laser off.

$A_\parallel = 2\pi \times 114.03$ MHz and $A_\perp = 2\pi \times 81.33$ MHz are, respectively, the longitudinal and transverse hyperfine parameters, and the z direction corresponds to the diamond $\langle 111 \rangle$ axis. When the externally applied magnetic field $\mathbf{B}$ is pointing close to a crystal direction $\langle 100 \rangle$, i.e., when $\cos^2\theta \simeq 1/3$, the electron spin resonance at angular frequency $\gamma_e B$ is split due to the interaction with the nuclear spin into three resonances, corresponding to three transitions, in which the nuclear spin magnetic quantum number is conserved. To first order in perturbation theory, the angular resonance frequencies are given by $\gamma_e B - \omega_{en}$, $\gamma_e B$, and $\gamma_e B + \omega_{en}$, where $\omega_{en}^2 = A_\parallel^2 \cos^2\theta + A_\perp^2 \sin^2\theta$. For the case where $\cos^2\theta = 1/3$, the calculated splitting is given by $\omega_{en}/2\pi = 93.5$ MHz, whereas the value extracted from the data seen in Fig. 4 is 93.82 MHz. The plots labeled F in Fig. 4 represent the theoretical prediction based on the analytical expressions (4), (6), and (7). The comparison with the CDMR data plots (labeled D) yields a good agreement. The parameters that have been employed for the calculation are listed in the figure caption.

VI. CONCLUSION

The nonlinearity in cavity response has an important impact on the sensitivity of spin detection. Let S_N be the minimum detectable change in the number of spins δN_s per a given square root of the available bandwidth (i.e., the inverse of the averaging time). It is assumed that sensitivity is limited by the fundamental bound imposed upon the signal-to-noise ratio by shot noise. When the cavity's response is linear, S_N is proportional to $E_c^{-1/2}$ (see Eq. (1) in [37]), and thus in this regime sensitivity can be enhanced by increasing the energy stored in the cavity $E_c\hbar\omega_c$. However, nonlinearity, which can be avoided only when $E_c \ll E_{cc}$ [see Eq. (4)], imposes a bound upon sensitivity enhancement. When the sensitivity coefficient S_N is calculated according to Eq. (1) in Ref. [37] for the case where the number of cavity photons is taken to be E_{cc} and the responsivity is calculated using Eq. (A2) below, one finds that S_N becomes

$$S_N \simeq \frac{2}{|P_{zST}|^{3/2}} \left(\frac{\gamma_c}{g_s^2} \frac{2T_1}{T_2} \right)^{1/2}. \tag{9}$$

Note that in general, $2T_1/T_2 \geqslant 1$ (see Eq. (A79) in [22]). For example, for the parameters of our device with laser off, Eq. (9) yields $S_N = 5 \times 10^7$ Hz$^{-1/2}$. The estimate given by Eq. (9) is expected to be applicable for any cavity-based technique of spin detection.

To conclude, in this work we have observed strong coupling (i.e., cooperativity larger than unity) between a superconducting microwave cavity and spin ensembles in diamond (the measured values of the cooperativity parameter $N_{eff} g_s^2/\gamma_c\gamma_2$ are 14 with the NV$^-$ ensemble and laser intensity of 30 mW mm^{-2} and 6.2 with the $P1$ ensemble). We find that the coupling imposes an upper bound upon the input microwave power, for which the cavity response remains linear. This bound has important implications for the sensitivity of traditional spin-detection protocols that are based on linear response. On the other hand, in some cases, nonlinearity can be exploited for sensitivity enhancement (e.g., by generating parametric amplification). However, further study is needed to explore ways of optimizing the performance of sensors operating in the nonlinear regime.

ACKNOWLEDGMENTS

We thank Adrian Lupascu for useful discussions. This work is supported by the Israeli Science Foundation and the Binational Science Foundation.

N.A. and S.M. contributed equally to this work.

APPENDIX: WEAK NONLINEARITY

In the weak nonlinear regime, it is assumed that the averaged number of cavity mode photons E_c is sufficiently small to allow one to take nonlinearity into account to lowest nonvanishing order only. In this limit, the cavity mode has a nonlinear response that can be adequately described using the well-known Duffing-Kerr model [38]. However, as is discussed below, when higher-order terms in E_c become significant, the response can no longer be described by the Duffing-Kerr model. The distinction becomes most pronounced in the limit of high-input microwave power. Both our experimental (see Figs. 3 and 4) and theoretical [see Eq. (4)] results indicate that the cavity mode becomes effectively decoupled from the spins in the limit of high microwave power. Consequently, linearity is restored at high-input power, provided that the input power is not made too high and is kept below the region where intrinsic cavity mode nonlinearity, which is characterized by the intrinsic Kerr coefficient K_c and intrinsic cubic damping rate G_c, becomes significant. Note that in our device, the intrinsic nonlinearity becomes noticeable only when the input power exceeds a value of about 0 dBm, which is 5–6 orders of magnitude higher than the value at which the cavity becomes effectively decoupled from the spins.

To first order in E_c, the spin-induced shift Υ_s in the complex cavity mode angular frequency can be expanded as

[see Eq. (4)]

$$\Upsilon_s = \omega_{cs} - i\gamma_{cs} + (K_{cs} - iG_{cs})E_c + O(E_c^2), \tag{A1}$$

where the shift in linear frequency ω_{cs} and the Kerr coefficient K_{cs} are given by

$$\omega_{cs} = \frac{N_{\rm eff} g_s^2}{\Delta} \frac{1}{1+\zeta_2^2}, \tag{A2}$$

$$K_{cs} = -\frac{N_{\rm eff} g_s^2}{\Delta E_{cc}} \left(\frac{\zeta_2}{1+\zeta_2^2}\right)^2, \tag{A3}$$

the linear damping rate is given by $\gamma_{cs} = \zeta_2 \omega_{cs}$, the cubic damping rate is given by $G_{cs} = \zeta_2 K_{cs}$, and where $\zeta_2 = 1/\Delta T_2$. In the regime of linear response (i.e., when $\Upsilon_s = \omega_{cs} - i\gamma_{cs}$), Eq. (A1) reproduces well-known results for spin-induced frequency shift and broadening of the cavity resonance [1]. The validity conditions for Eqs. (4) and (A1) are discussed in Ref. [22].

In general, in the weak nonlinear regime, in which higher-order terms in E_c can be disregarded, the terms proportional to E_c in the complex angular frequency shift Υ_s [see Eq. (A1)] may give rise to bistability in the response of the system to an applied monochromatic driving. At the onset of bistability, the averaged number E_c obtains a value denoted by E_{co}. When the value of E_{co} is estimated based on the assumption that higher-order terms in E_c may be disregarded, one finds for the parameters of our device that $E_{co} \simeq 2E_{cc}$ (calculated using Eq. (42) in Ref. [25]). On the other hand, the assumption that higher-order terms in E_c may be disregarded is applicable only when $E_c \ll E_{cc}$, and thus the nonlinearity cannot be considered as weak in this region. When the bistability is accessible, the system can be used for signal amplification [38], which can yield a significant gain close to the onset of bistability [25].

[1] S. Haroche and D. Kleppner, Phys. Today **42**(1), 24 (1989).
[2] A. Wallraff, D. I. Schuster, A. Blais, L. Frunzio, R.-S. Huang, J. Majer, S. Kumar, S. M. Girvin, and R. J. Schoelkopf, Nature (London) **431**, 162 (2004).
[3] J. Anders, in *Recent Advances in Nonlinear Dynamics and Synchronization* (Springer-Verlag, Berlin, Heidelberg, 2018), pp. 57–87.
[4] N. Maleeva, M. V. Fistul, A. Karpov, A. P. Zhuravel, A. Averkin, P. Jung, and A. V. Ustinov, J. Appl. Phys. **115**, 064910 (2014).
[5] X. Zhu, S. Saito, A. Kemp, K. Kakuyanagi, S.-i. Karimoto, H. Nakano, W. J. Munro, Y. Tokura, M. S. Everitt, K. Nemoto *et al.*, Nature (London) **478**, 221 (2011).
[6] Y. Kubo, F. Ong, P. Bertet, D. Vion, V. Jacques, D. Zheng, A. Dréau, J.-F. Roch, A. Auffèves, F. Jelezko *et al.*, Phys. Rev. Lett. **105**, 140502 (2010).
[7] Y. Kubo, C. Grezes, A. Dewes, T. Umeda, J. Isoya, H. Sumiya, N. Morishita, H. Abe, S. Onoda, T. Ohshima *et al.*, Phys. Rev. Lett. **107**, 220501 (2011).
[8] R. Amsüss, C. Koller, T. Nöbauer, S. Putz, S. Rotter, K. Sandner, S. Schneider, M. Schramböck, G. Steinhauser, H. Ritsch *et al.*, Phys. Rev. Lett. **107**, 060502 (2011).
[9] D. Schuster, A. Sears, E. Ginossar, L. DiCarlo, L. Frunzio, J. Morton, H. Wu, G. Briggs, B. Buckley, D. Awschalom *et al.*, Phys. Rev. Lett. **105**, 140501 (2010).
[10] K. Sandner, H. Ritsch, R. Amsüss, C. Koller, T. Nöbauer, S. Putz, J. Schmiedmayer, and J. Majer, Phys. Rev. A **85**, 053806 (2012).
[11] C. Grezes, B. Julsgaard, Y. Kubo, M. Stern, T. Umeda, J. Isoya, H. Sumiya, H. Abe, S. Onoda, T. Ohshima *et al.*, Phys. Rev. X **4**, 021049 (2014).
[12] D. Farfurnik, N. Alfasi, S. Masis, Y. Kauffmann, E. Farchi, Y. Romach, Y. Hovav, E. Buks, and N. Bar-Gill, Appl. Phys. Lett. **111**, 123101 (2017).
[13] M. W. Doherty, N. B. Manson, P. Delaney, F. Jelezko, J. Wrachtrup, and L. C. Hollenberg, Phys. Rep. **528**, 1 (2013).
[14] J. Maze, A. Gali, E. Togan, Y. Chu, A. Trifonov, E. Kaxiras, and M. Lukin, New J. Phys. **13**, 025025 (2011).
[15] J. Wrachtrup and F. Jelezko, J. Phys.: Condens. Matter **18**, S807 (2006).
[16] P. Ovartchaiyapong, K. W. Lee, B. A. Myers, and A. C. B. Jayich, Nat. Commun. **5**, 4429 (2014).
[17] E. R. MacQuarrie, T. A. Gosavi, N. R. Jungwirth, S. A. Bhave, and G. D. Fuchs, Phys. Rev. Lett. **111**, 227602 (2013).
[18] L. Rondin, J. Tetienne, T. Hingant, J. Roch, P. Maletinsky, and V. Jacques, Rep. Prog. Phys. **77**, 056503 (2014).
[19] A. Gruber, A. Dräbenstedt, C. Tietz, L. Fleury, J. Wrachtrup, and C. Von Borczyskowski, Science **276**, 2012 (1997).
[20] D. Le Sage, L. M. Pham, N. Bar-Gill, C. Belthangady, M. D. Lukin, A. Yacoby, and R. L. Walsworth, Phys. Rev. B **85**, 121202 (2012).
[21] M. Boissonneault, J. M. Gambetta, and A. Blais, Phys. Rev. A **77**, 060305 (2008).
[22] E. Buks, C. Deng, Jean-Luc F. X. Orgazzi, M. Otto, and A. Lupascu, Phys. Rev. A **94**, 033807 (2016).
[23] M. Loretz, H. Takahashi, T. F. Segawa, J. M. Boss, and C. L. Degen, Phys. Rev. B **95**, 064413 (2017).
[24] T.-L. Wee, Y.-K. Tzeng, C.-C. Han, H.-C. Chang, W. Fann, J.-H. Hsu, K.-M. Chen, and Y.-C. Yu, J. Phys. Chem. A **111**, 9379 (2007).
[25] B. Yurke and E. Buks, J. Lightwave Tech. **24**, 5054 (2006).
[26] M. Drake, E. Scott, and J. Reimer, New J. Phys. **18**, 013011 (2015).
[27] L. Robledo, H. Bernien, T. van der Sar, and R. Hanson, New J. Phys. **13**, 025013 (2011).
[28] D. A. Redman, S. Brown, R. H. Sands, and S. C. Rand, Phys. Rev. Lett. **67**, 3420 (1991).
[29] J. Harrison, M. Sellars, and N. Manson, Diam. Relat. Mater. **15**, 586 (2006).
[30] C. S. Shin, C. E. Avalos, M. C. Butler, D. R. Trease, S. J. Seltzer, J. P. Mustonen, D. J. Kennedy, V. M. Acosta, D. Budker, A. Pines *et al.*, J. Appl. Phys. **112**, 124519 (2012).
[31] K. Jensen, V. M. Acosta, A. Jarmola, and D. Budker, Phys. Rev. B **87**, 014115 (2013).
[32] W. Kaiser and W. Bond, Phys. Rev. **115**, 857 (1959).
[33] W. Smith, P. Sorokin, I. Gelles, and G. Lasher, Phys. Rev. **115**, 1546 (1959).

[34] J. Loubser and J. van Wyk, Rep. Prog. Phys. **41**, 1201 (1978).

[35] J. D. A. Wood, D. A. Broadway, L. T. Hall, A. Stacey, D. A. Simpson, J.-P. Tetienne, and L. C. L. Hollenberg, Phys. Rev. B **94**, 155402 (2016).

[36] E. Reynhardt, G. High, and J. Van Wyk, J. Chem. Phys. **109**, 8471 (1998).

[37] E. Buks, S. Zaitsev, E. Segev, B. Abdo, and M. P. Blencowe, Phys. Rev. E **76**, 026217 (2007).

[38] A. Roy and M. Devoret, C. R. Phys. **17**, 740 (2016).